ACS OMEGA

Open Access

http://pubs.acs.org/journal/acsodf

Article

Hydrolysis of Carbonyl Sulfide in Blast Furnace Gas Using Alkali Metal-Modified γ-Al_2O_3 Catalysts with High Sulfur Resistance

Qiang Cao, Yuting Lin, Yuran Li,* Jinglei Tian, Hongqiang Liu, Tingyu Zhu, and Jiancheng Wang

Cite This: *ACS Omega* 2023, 8, 35608−35618

Read Online

ACCESS | Metrics & More | Article Recommendations

ABSTRACT: A carbonyl sulfide (COS) hydrolysis catalyst can play an efficient role in blast furnace gas (BFG), but the life of the catalyst is greatly shortened due to the presence of O_2 and H_2S in the atmosphere, so improving the sulfur resistance of the catalyst is the key to application. In this work, alkali metals Na and K modified γ-Al_2O_3 catalysts to improve COS hydrolysis efficiency and sulfur resistance by adding an alkaline center. Compared with γ-Al_2O_3 catalysts, the COS hydrolysis efficiency of the modified catalysts in the experiment was improved by 12% in the presence of H_2S and O_2. The main cause of catalyst sulfur poisoning is the presence of O_2, which intensifies both the total amount of sulfur deposition and the proportion of sulfate. It is found that the NaOH/Al_2O_3 catalyst shows better sulfur resistance than the KOH/Al_2O_3 catalyst for two reasons: first, the support of Na can significantly improve the medium-strong alkaline site, which is the adsorption site of H_2S. This is equivalent to increasing the "sulfur capacity" of H_2S adsorption and reducing the impact of sulfur deposition on the main reaction. Second, the elemental sulfur is more easily produced on the NaOH/Al_2O_3 catalyst, but the sulfur is further oxidized to sulfate and sulfite on the KOH/Al_2O_3 catalyst. The molecular diameter of elemental sulfur is smaller than that of sulfate. Therefore, the NaOH/Al_2O_3 catalyst has better sulfur resistance.

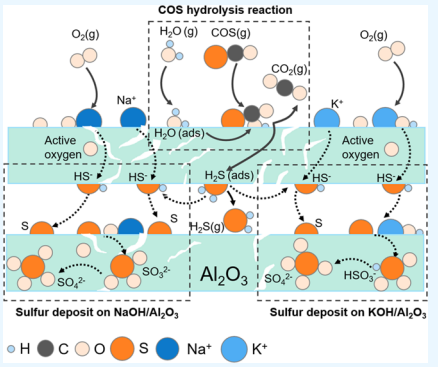

1. INTRODUCTION

The blast furnace iron-making process accounts for 70% of the total carbon emissions of the whole steel process with the implementation of reducing pollution and carbon emissions in China.[1−5] The blast furnace gas (BFG) desulfurization facilities are necessary before the carbon capture, utilization, and storage (CCUS) process since the existence of sulfur will cause the deactivation of the carbon capture catalyst.[6−8] According to the online test results from HBIS Group, Tangshan, Hebei Province, China in 2022, COS concentration is 150−450 mg/m^3, H_2S concentration is 80−150 mg/m^3, O_2 concentration is 0.1−0.6 vol %, and H_2O concentration is 5−10 vol %. The total sulfur content in BFG is about 150−400 mg/m^3, of which more than 80% is carbonyl sulfide (COS), and the rest is hydrogen sulfide (H_2S).[9,10] The properties of COS are stable, and the removal methods include a catalytic hydrogenation method, a catalytic hydrolysis method, an alcohol amine adsorption method,[11] and a combustion method, in which SO_2 is generated and removed by direct combustion and oxidation, as given in eqs 1−4.

$$COS + H_2 \rightarrow H_2S + CO \quad (1)$$

$$COS + H_2O \rightarrow H_2S + CO_2 \quad (2)$$

$$COS + RNH_2 \rightarrow RNH_2^+COS^- \quad (3)$$

$$2COS + 3O_2 \rightarrow 2SO_2 + 2CO_2 \quad (4)$$

The catalytic hydrolysis method is selected for the blast furnace gas desulfurization due to the low desulfurization temperature (100−150 °C), low COS concentration (150−450 mg/m^3), and containing water vapor (5−8%). The H_2O vapor in the gas can be used as the reaction gas, and the original H_2S in the gas and the H_2S product can be removed together.[12] COS hydrolysis is an alkali-catalyzed reaction on a catalyst, as given in eq 2. γ-Al_2O_3 is an amphoteric oxide with both acidic and alkaline sites.[13−17] Although COS hydrolysis catalyst can play an efficient role in BFG, the life of the catalyst is greatly shortened due to the presence of O_2 and H_2S in the atmosphere, so improving the sulfur resistance of the catalyst is the key to application.

Previous studies have shown that the alkaline center is the active center of the COS hydrolysis reaction.[12,20] The alkalinity of the catalyst surface can be adjusted to accelerate the reaction rate.[18,19] The alkaline sites on the surface of γ-Al_2O_3 catalyst are divided into three kinds of sites: strong alkaline sites, medium-strong alkaline sites, and weak alkaline sites.[21−23]

Received: March 17, 2023
Accepted: July 3, 2023
Published: September 18, 2023

When the total alkalinity ($H_0 = pK_a = -\lg K_a$) of the hydrolysis catalyst is 4.8−9.8, it can obviously promote hydrolysis; while if the total alkalinity is too high or too low, it will play an opposite role.[12,24] Currently, there are many theories on COS hydrolysis reaction, including the alkali catalysis mechanism, Eley−Kideal mechanism, thiocarbonate intermediate mechanism, etc. It is generally believed that COS adsorbs on the γ-Al_2O_3 surface to form hydrated COS and further interacts with −OH or adsorbed H_2O to generate CO_2 and H_2S.[25−31] These theories are usually based on clean gas with low O_2 less than 0.1%. The content of O_2 ranging from 0.1 to 0.3% in BFG is higher than that in water gas used for COS hydrolysis catalyst at present. Therefore, research on the interaction between COS and the alkaline center of catalyst in the presence of O_2 is urgently needed.

The results of the pilot-scale plant for BFG desulfurization show that the service life of conventional γ-Al_2O_3 is less than 3 months far from the demand of 2 years. The deactivation of the hydrolysis catalyst mainly comes from the deposition of sulfur-containing products on the catalyst surface.[32,33] H_2S can be oxidized to produce sulfur deposition. The type and amount of deposition products are closely related to the content of H_2S and O_2 and reaction temperature, as well as the intensity of alkaline sites on the catalyst surface.[33,34] Increasing the alkalinity of the hydrolysis catalyst by supporting alkali metals is an important way to improve the sulfur resistance of the catalyst.[35] The modification of alkali metal can effectively increase the alkaline sites on the catalyst surface, but the mechanism of the modified catalysts on H_2S and O_2 is still unclear, so it is necessary to systematically study the sulfur-resistant mechanism of the COS hydrolysis catalyst.

CO_2 has an inhibitory effect on the hydrolysis reaction of COS due to its acidity. Carbon accumulation also is one of the main causes of catalyst deactivation. In order to provide a clearer explanation for the influence of sulfur deposition on the hydrolysis reaction, only COS, H_2S, H_2O, and O_2 were introduced in the complex atmosphere.

In this work, the alkali metal-modified γ-Al_2O_3 was designed and prepared. The effect of alkali sites on COS hydrolysis activity was investigated, and the hydrolysis efficiency was improved by controlling the alkali sites of the catalyst. The effect mechanism of H_2S and O_2 on the sulfur deposition was revealed, which helps to improve the sulfur resistance of the catalyst.

2. EXPERIMENTAL SECTION

2.1. Catalyst Preparation. NaOH, Na_2CO_3, CH_3COONa, KOH, K_2CO_3, and CH_3COOK-modified γ-Al_2O_3 catalysts with a mass fraction of 3% (calculated according to the mass of alkali metal) were prepared by the impregnation method. All reagents are of analytical grade and from Sinopharm Chemical Reagent Co., Ltd. with analytical purity. The specific preparation steps are as follows: 0.052 g of NaOH, 0.069 g of Na_2CO_3, 0.107 g of CH_3COONa, 0.043 g of KOH, 0.053 g of K_2CO_3, 0.075 g of CH_3COOK, and 1 g of γ-Al_2O_3 (0.25−0.83 nm) were accurately weighed, and then, 10 mL of distilled water was added and stirred for 1 h to make them fully and evenly mixed. Then, excess water was removed by rotating evaporation. After spinning, the sample was put into an oven at 120 °C and dried at a constant temperature for 12 h. The dried samples were calcined at 500 °C for 5 h in a muffle furnace to obtain the hydrolysis catalysts NaOH/Al_2O_3, Na_2CO_3/Al_2O_3, CH_3COONa/Al_2O_3, KOH/Al_2O_3, K_2CO_3/Al_2O_3, and CH_3COOK/Al_2O_3.

2.2. Characterization. The surface ratio of metal elements to total metal elements was characterized by X-ray fluorescence (XRF, PW4400/40, PANalytical B.V., the Netherlands). Inductively coupled plasma atomic emission spectroscopy (ICP-AES, OPTIMA 7000DV, PerkinElmer) was used to characterize the bulk ratio of metal content to total element content in the samples. For each test, samples were added to nitric acid for digestion until the metal ions were completely dissolved in the nitric acid solution.

The total alkali content of the catalyst was determined by Boehm titration. First, 0.5 g of samples were soaked in 50 mL of 0.1 mol/L HCl solutions, stirred for 24 h, filtered, and then fully washed. 10 mL of the filtrate was titrated with calibrated 0.1 mol/L NaOH solutions, and bromocresol green-methyl orange was used as an indicator to obtain the total base amount of catalyst according to the amount of NaOH solution and HCl solution.

An automatic specific surface area and porosity analyzer (NOVA3200e, Quantachrome) was used to detect the pore structure. The specific surface area was calculated using a multipoint Brunauer−Emmett−Teller (BET) equation. When $p/p_0 = 0.95$, the total pore volume (V_T) is determined by the nitrogen adsorption capacity at 77 K.

The surface morphology was characterized by scanning electron microscopy (SEM, SU8020, Hitachi, Japan), accompanied by energy-dispersive X-ray energy spectroscopy (EDX) and elemental mapping. The sample particles after sputtering gold were evenly dispersed on the conductive adhesive and magnified 5000 times for observation.

X-ray photoelectron spectrometry (XPS, ESCALAB 250Xi, Thermo Fisher) was used to test metal valence states with Al Kα rays at 15 kV and 10 mA. The test pass energy was 50 eV with a step size of 0.05 eV, and the combined energy standard C 1s at 284.80 eV was used for charge correction.

The basic center on the catalyst was characterized by CO_2 temperature-programmed desorption (CO_2-TPD) using a chemical adsorption apparatus (AutoChem II2920, Micromeritics). An 80 mg sample was adsorbed in a CO_2 atmosphere with a 30 mL/min air flow rate at 50 °C for 30 min, pretreated in N_2 at 200 °C for 2 h, and finally desorbed in N_2 at a heating rate of 5 °C/min to 800 °C. Based on the CO_2-TPD curves, the content of corresponding alkaline centers could be obtained by integrating the area of the curves at a given temperature window.

The total weight loss caused by sulfur desorption was measured by thermogravimetric analysis (TG, DTG-60H, Shimadzu, Japan). 1.0 g of sample was adsorbed in 100 mL/min mixture gas with 140 mg/m^3 H_2S and a balance of He, at 50 °C for 2 h, and then, temperature-programmed desorption was performed in a He atmosphere at a heating rate of 10 °C/min. The final desorption temperature was 900 °C.

The gas from the outlet of the reaction tube entered the mass spectrum (MS, GAM200, InProcess Instruments, Germany) through the capillary sample tube. The vacuum degree of the mass spectrum was maintained at 10^{-7} Pa, and the voltage of the electron multiplier was 1390 V. The MID method was used to continuously monitor the changes of signals with the mass/charge ratio (m/z).

In situ diffuse reflectance infrared Fourier transform (in situ DRIFT) spectra were collected from the 1000−4000 cm^{-1} wavenumber range using the ZnSe window on an FTIR

https://doi.org/10.1021/acsomega.3c01811
ACS Omega 2023, 8, 35608−35618

spectrometer (Nicolet 6700, Thermal). The IR spectra were recorded at a spectral resolution of 4 cm^{-1}.

2.3. Activity Tests. The hydrolysis activity of COS on the catalyst was evaluated in a quartz fixed bed reactor with an inner diameter of 6 mm under atmospheric pressure. Test conditions included a reaction temperature of 120 °C, gas flow rate of 300 mL/min, and gas hourly space velocity (GHSV) of 220 000 h^{-1}. The gas mixture contained 400 mg/m^3 COS, 140 mg/m^3 H_2S (if used), 7 vol % H_2O, and 0.3 vol % O_2 (if used), with a balance of N_2. Water vapor was brought into the reaction atmosphere using a water vapor generator controlled by N_2 through a constant temperature water bath. All of the pipes were heated at 80 °C to prevent water vapor condensation. A gas chromatography analyzer (GC, GC-2010PLUS, Shimadzu, Japan) was used to detect the outlet concentrations of COS and H_2S. The hydrolysis efficiency of COS is shown in eq 5

$$\text{COS conversion} = \frac{C_{in} - C_{out}}{C_{in}} \times 100\% \quad (5)$$

where C_{in} is the inlet concentration of COS, mg/m^3, and C_{out} is the outlet concentration of COS, mg/m^3.

The amount of sulfur deposited on the catalyst surface is given in eq 6

$$H_2S \text{ deposition} = \frac{MQ\int_0^t (C_{in-S} - C_{out-S})dt}{m} \times 60 \quad (6)$$

H_2S deposition is the amount of sulfur deposited on 1 g of catalyst, mg/g. $C_{in\text{-}S}$ is the total concentration of S mg/m^3, $C_{out\text{-}S}$ is the outlet concentration of S, mg/m^3, t is the reaction time, h, M is the atomic mass of a sulfur element, g/mol, Q is the gas flow rate, mL/min, and m is the catalyst amount, g.

3. RESULTS AND DISCUSSION

3.1. Precursors on COS Hydrolysis Catalysts. In order to screen COS hydrolysis catalysts with higher activity, ICP and XRF tests were conducted on samples prepared from different precursors, and the results are shown in Table 1. The

Table 1. Content of Metal Load (wt %) and Total Alkalinity of Catalyst (mmol/g)

samples	actual metal load (wt %)		total alkalinity (mmol/g)
	ICP	XRF	
γ-Al_2O_3			7.21
$NaOH/Al_2O_3$	2.82	4.31	9.76
Na_2CO_3/Al_2O_3	2.67	4.30	9.45
CH_3COONa/Al_2O_3	2.12	3.81	9.01
KOH/Al_2O_3	2.89	5.24	9.92
K_2CO_3/Al_2O_3	2.74	4.44	9.55
CH_3COOK/Al_2O_3	2.14	3.90	9.11

actual loading content of alkali metals on γ-Al_2O_3 supports follows the order: MOH > MCO_3 > CH_3COOM (M stands for K or Na), consistent with the alkaline sequence of precursors. The metal loading amount obtained by the XRF test is much larger than that by the ICP test because XRF tests the surface phase of the catalyst, while ICP tests the bulk phase of the catalyst, showing that the loading of alkali metal is mostly concentrated on the surface of the catalyst. After the alkali metal is supported, the total alkalinity of all of the catalysts is significantly increased by about 25−38%, and the total alkalinity of the catalysts supported by Na and K both conform to the characteristics of MOH > MCO_3 > CH_3COOM, which is also positively related to the alkalinity of the precursor. And then, the alkalinity of the catalysts loaded with K is also slightly higher than that of the catalysts loaded with Na. The loading content of K is slightly higher than that of Na due to the higher alkalinity of K. Therefore, all samples can be regarded as successfully loaded with corresponding alkali metals.

The hydrolysis efficiency of COS on various catalysts was investigated, and the results are shown in Figure 1. The

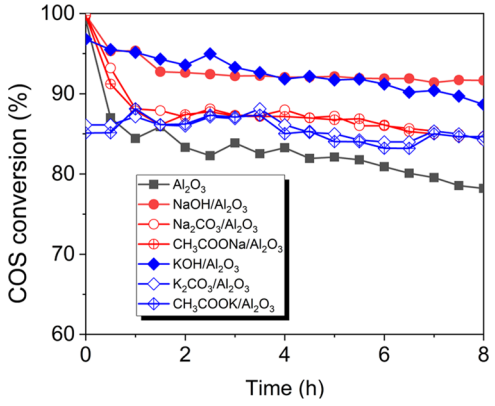

Figure 1. COS hydrolysis efficiency on various catalysts.

hydrolysis efficiency of COS on $NaOH/Al_2O_3$ and KOH/Al_2O_3 significantly increased up to 90% during the 8 h reaction time. The other four alkali metal-supported catalysts have no obvious difference in the COS hydrolysis efficiency, but the efficiency is about 7% higher than 80% of γ-Al_2O_3. The COS hydrolysis efficiency on KOH/Al_2O_3 is higher in the early stage but gradually decreases close to that on $NaOH/Al_2O_3$, indicating that the two catalysts may have different mechanisms of COS hydrolysis. Based on Figure 1 and Table 1, it can be concluded that COS hydrolysis efficiency has no positive relationship with the total alkalinity. It may be related to the type of alkaline center. In view of the excellent COS hydrolysis efficiency of $NaOH/Al_2O_3$ and KOH/Al_2O_3 catalysts with high total alkalinity, these two catalysts were used in subsequent analysis.

The hydrolysis efficiency on 2−5 mm spherical γ-Al_2O_3 catalyst was only 51% when the initial concentration of COS ranged in 84−110 mg/m^3 at atmospheric pressure, 200 °C, and gas hourly space velocity of 3000 h^{-1}.[36,36] The hydrolysis efficiency was ∼91% at the initial COS concentration of 200 ppm, 120 °C, and gas hourly space velocity of 2400 h^{-1} with 5% NaOH supported by Al/Ti.[37] In this work, the COS concentration and the gas hourly space velocity are higher, and the hydrolysis efficiency can still reach about 90% after 8 h reaction time. Therefore, the prepared catalyst in this work has an excellent hydrolysis performance.

3.2. Alkali Sites of COS Hydrolysis on the Catalysts. The pore size distribution and specific surface area of γ-Al_2O_3, $NaOH/Al_2O_3$, and KOH/Al_2O_3 catalysts before and after the COS hydrolysis reaction are shown in Figure 2. The pore size of the three catalysts mainly ranges from 3 to 50 nm. The most probable pore size is 7−10 nm, and the proportion increases significantly after metal loading. The developed pore structure

https://doi.org/10.1021/acsomega.3c01811
ACS Omega 2023, 8, 35608−35618

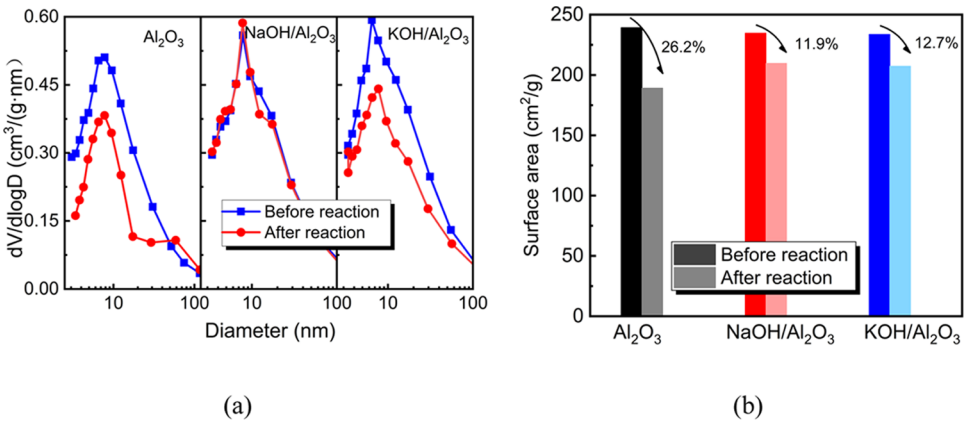

Figure 2. (a) Pore size distribution and (b) specific surface area and total pore volume of catalysts.

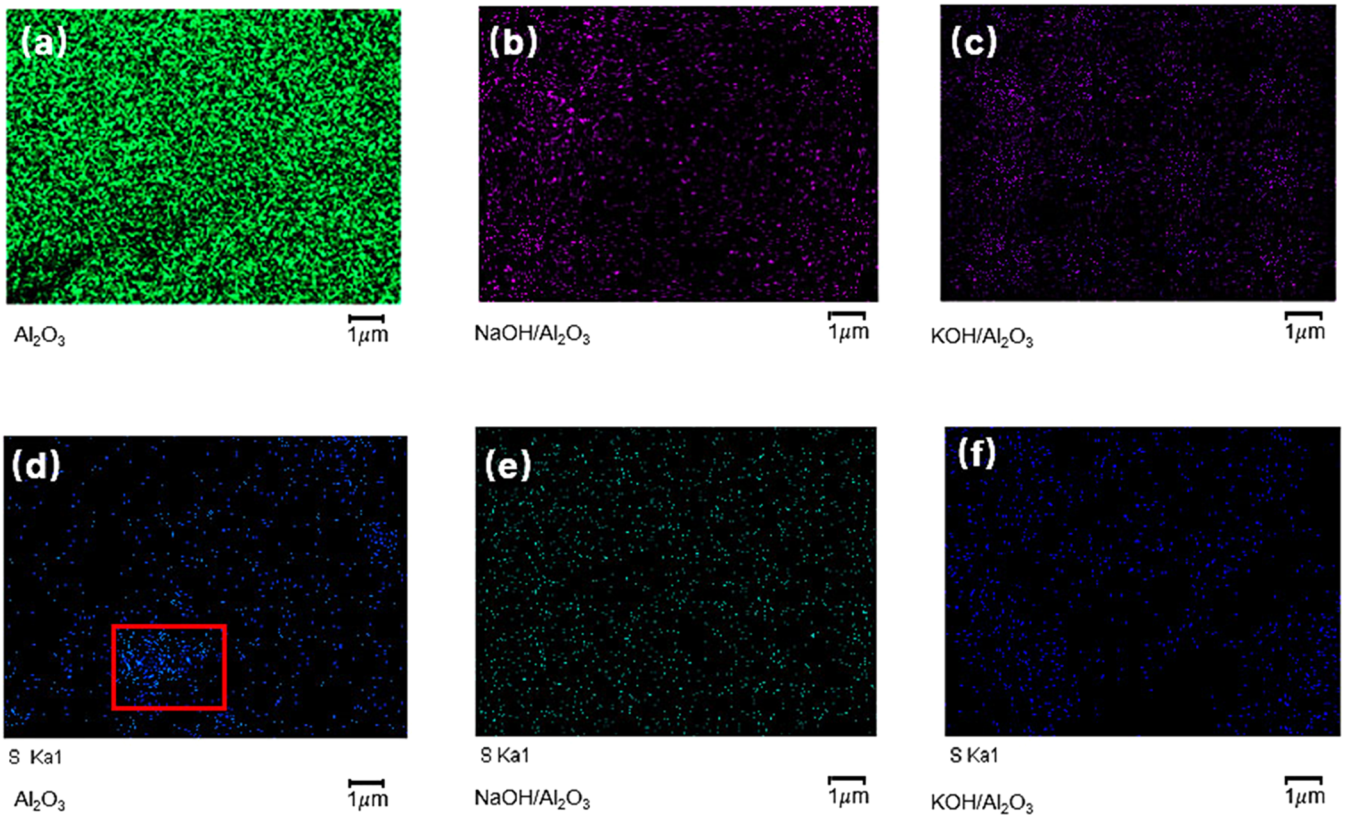

Figure 3. Mapping images of catalysts before and after reaction for γ-Al_2O_3, $NaOH/Al_2O_3$, and KOH/Al_2O_3 catalysts ((a) Al element in γ-Al_2O_3; (b) Na element in $NaOH/Al_2O_3$; (c) K element in KOH/Al_2O_3; (d) S element in γ-Al_2O_3; (e) S element in $NaOH/Al_2O_3$; and (f) S element in KOH/Al_2O_3).

is more conducive to the adsorption of COS and promotes the mass transfer process. The specific surface area of the catalyst decreases only by about 2% due to the metal loading, so this effect is negligible. The changes of the pore structure before and after the reaction is more obvious. The specific surface area of KOH/Al_2O_3 decreases by 12.7% after the reaction, and the proportion of the most probable pore size decreases by 27.0%. Although the specific surface area of $NaOH/Al_2O_3$ also decreases by 11.9%, the proportion of the most probable pore size is almost unchanged. The results further indicate that the types of reaction products or deposition sites of $NaOH/Al_2O_3$ and KOH/Al_2O_3 catalysts are different.

The SEM surface morphology of γ-Al_2O_3, $NaOH/Al_2O_3$, and KOH/Al_2O_3 catalysts is shown in Figure 3. The metal components Na and K are uniformly distributed on the catalyst surface. After the COS hydrolysis reaction, the sulfur element is deposited on the catalyst surface, and some sulfur aggregated on the γ-Al_2O_3 surface. The sulfur deposition on the $NaOH/Al_2O_3$ and KOH/Al_2O_3 surface is more uniform, which may be caused by the increase of hydrolysis active sites due to the load of alkali metals.

To explore the role of alkaline centers on the catalysts, CO_2-TPD was used to characterize the distribution of alkaline centers. The results are shown in Figure 4. Three obvious CO_2 desorption peaks can be seen from the CO_2-TPD curve. The temperature of the first desorption peak is 50−200 °C, which belongs to the weak alkaline site and comes from the −OH group. The temperature of the second desorption peak is 200−

https://doi.org/10.1021/acsomega.3c01811
ACS Omega 2023, 8, 35608−35618

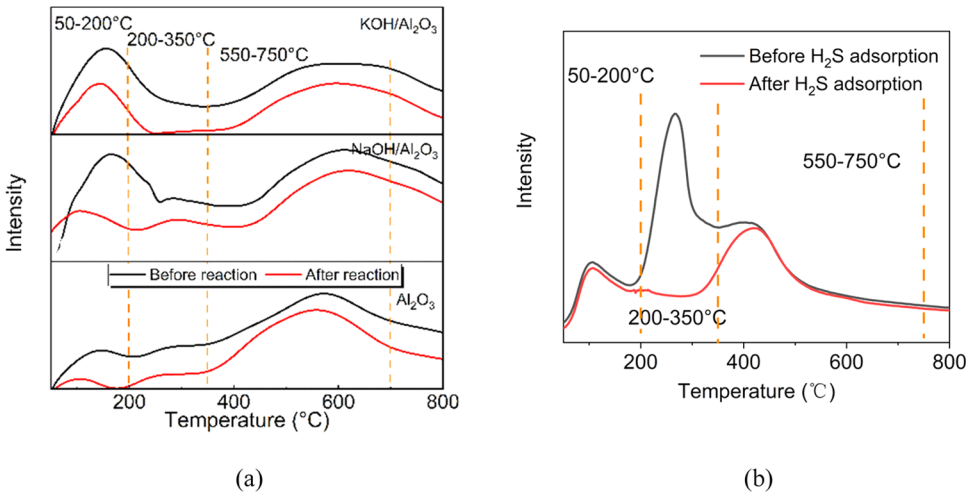

Figure 4. (a) CO_2-TPD curves of catalysts before and after reaction of COS hydrolysis and (b) H_2S adsorption on γ-Al_2O_3 loading with 8% NaOH.

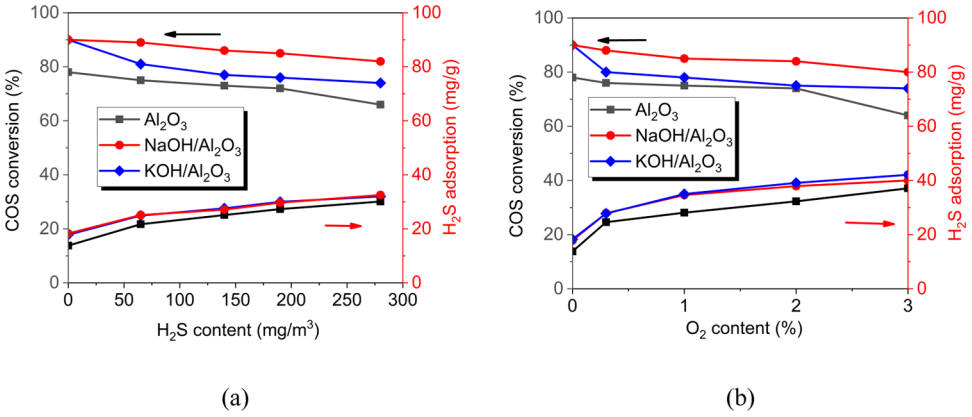

Figure 5. COS hydrolysis efficiency and H_2S adsorption under different (a) H_2S contents and (b) O_2 contents.

350 °C, which belongs to the medium-strong alkaline site and comes from the M−O group. The temperature of the third desorption peak is 550−700 °C, which belongs to the strong alkaline site and comes from the O^{2-} group.[38−40] Compared with γ-Al_2O_3, the weak, medium-strong, and strong alkaline centers on the NaOH/Al_2O_3 catalyst increased by 62, 42, and 24%, respectively; for the KOH/Al_2O_3 catalyst, the corresponding volume is 53, 1, and 18%. Therefore, the loading of Na increased three kinds of alkaline centers, while the loading of K only increased the weak alkaline centers but reduced strong alkaline centers with unchanged medium-strong alkaline centers. It is generally believed that the weak alkaline centers are the active centers of COS hydrolysis.[12] The support of K and Na greatly increases the weak alkaline center on the catalyst, so the hydrolysis efficiency of COS has been significantly increased.

After hydrolysis, the weak, medium-strong, and strong alkaline centers on the surface of γ-Al_2O_3 decreased by 84, 68, and 28%, respectively; decreased by 57, 52, and 24% on NaOH/Al_2O_3, respectively; decreased by 46, 88, and 34% on KOH/Al_2O_3, respectively. The weak and medium-strong alkaline centers of the three catalysts simultaneously decreased. The weak alkaline center is the reaction site of COS hydrolysis, and it can be inferred that the medium-strong alkaline center is the H_2S adsorption site. The CO_2-TPD curve after H_2S adsorption was detected with results shown in Figure 4b. After H_2S adsorption, the medium-strong alkaline centers on γ-Al_2O_3 and KOH/Al_2O_3 catalysts are almost exhausted, and the efficiency of COS on the two catalysts declines significantly over time, while the efficiency of COS on NaOH/Al_2O_3 is relatively stable. It is speculated that the amount of medium-strong alkaline center is greatly increased by the support of Na. At the same time, it is mainly elemental sulfur deposited on the surface of NaOH/Al_2O_3, so the deposition of elemental sulfur has little impact on the NaOH/Al_2O_3 compared with γ-Al_2O_3 and KOH/Al_2O_3. The sulfur deposition includes the deposition of elemental sulfur and sulfate deposition; one of the main causes of catalyst poisoning is from the sulfate deposition, so the influence of the deposition of elemental sulfur is small. The NaOH/Al_2O_3 catalyst can maintain high activity for a long time, which is significantly different from KOH/Al_2O_3.

3.3. Sulfur-Containing Products in the Presence of H_2S and O_2. The main components affecting COS hydrolysis are H_2S and O_2. H_2S can also be oxidized by O_2 in the gas in addition to being oxidized by the alkaline center on the catalyst surface. The influence of O_2 and H_2S content on COS hydrolysis efficiency and H_2S adsorption was explored, and the results are shown in Figure 5.

The hydrolysis efficiency of COS was the highest in the absence of H_2S, which were 78, 90, and 90% on γ-Al_2O_3, NaOH/Al_2O_3, and KOH/Al_2O_3 catalysts, respectively. With the increase of H_2S concentration, the hydrolysis efficiency of COS decreases linearly. The decrease of efficiency on NaOH/

https://doi.org/10.1021/acsomega.3c01811
ACS Omega 2023, 8, 35608−35618

Al_2O_3 and KOH/Al_2O_3 catalysts is significantly smaller than that on γ-Al_2O_3, indicating that alkali metal modification improves the antisulfur poisoning ability of the catalysts. However, with the increase of H_2S concentration, the adsorption amount of H_2S in the three catalysts increases significantly, and sulfur deposition on the samples after alkali metal loading is more obvious than that on γ-Al_2O_3. This is because alkali metal loading increased the alkalinity of the catalyst, so more H_2S is adsorbed. However, the hydrolysis efficiency of COS is only slightly reduced because the increase of alkaline centers can partially offset the negative effects caused by sulfur deposition.

From Figure 5b, the existence of O_2 has a significant inhibition on the hydrolysis efficiency of COS. The efficiency of COS hydrolysis on γ-Al_2O_3, $NaOH/Al_2O_3$, and KOH/Al_2O_3 catalysts decreased by 18, 11, and 18%, respectively, when the O_2 concentration increased from 0 to 3%. The amount of H_2S adsorption in the presence of O_2 is significantly increased compared with that in the absence of O_2. The alkali metal loading increases the sulfur deposition, and there is little difference between $NaOH/Al_2O_3$ and KOH/Al_2O_3. The difference of COS hydrolysis efficiency on $NaOH/Al_2O_3$ and KOH/Al_2O_3 may be from the sulfur species.

In order to determine the sulfur deposition form, sulfur species on catalysts after the COS hydrolysis reaction were investigated through XPS. The sulfur element distribution diagram is shown in Figure 6. The sulfur element 2p peak was

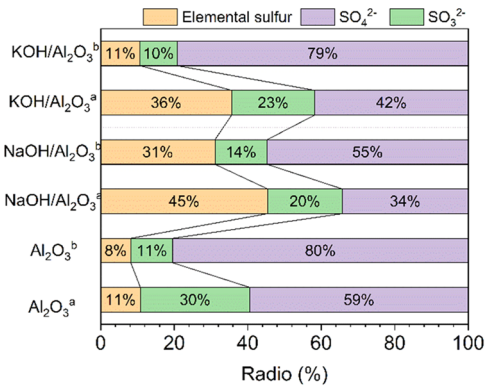

Figure 6. Sulfur element distribution diagram after the COS hydrolysis reaction for various catalysts ([a] in COS + H_2O, [b] in COS + H_2O + 0.3% O_2).

decomposed into three peaks: elemental sulfur (163.90−165.60 eV, S $2p_{3/2}$ and S $2p_{1/2}$), SO_3^{2-} (166.40−167.00 eV), and SO_4^{2-} (167.00−168.50 eV).[11] Before the reaction, there is no sulfur component on the catalyst. After the reaction, SO_3^{2-} and SO_4^{2-} are the main forms of sulfur deposition on the catalyst surface, accompanied by elemental sulfur. Compared with γ-Al_2O_3, the content of sulfate species on $NaOH/Al_2O_3$ and KOH/Al_2O_3 catalysts decreased significantly, but the content of elemental sulfur increased, indicating that the alkali metal loading inhibited the oxidation of H_2S on the catalyst surface, making more sulfur elements deposited on the catalyst surface in the form of elemental sulfur. Since the volume of sulfate (76.9 cm^3/mol) per mole is larger than that of elemental sulfur (13.6 cm^3/mol), this may be the reason why the specific surface area of γ-Al_2O_3 catalyst, as shown in Figure 2b, decreases more significantly after the reaction. $NaOH/Al_2O_3$ has more elemental sulfur than the KOH/Al_2O_3 catalyst, which is also mutually verified by the pore size distribution of both. In the presence of O_2, the sulfate increases greatly by up to 37%, especially on KOH/Al_2O_3, which is an important reason why O_2 inhibits the hydrolysis of COS. The presence of O_2 increases the oxidation of sulfur to generate the sulfate deposition on catalysts, covering the active site, which greatly reduces the hydrolysis efficiency. However, $NaOH/Al_2O_3$ still has a certain proportion of elemental sulfur, and the proportion of sulfate is smaller on $NaOH/Al_2O_3$ than that on γ-Al_2O_3 and KOH/Al_2O_3. The molecular diameter of elemental sulfur is smaller than that of sulfate, so it has less inhibition on COS hydrolysis, which is consistent with the higher hydrolysis efficiency on $NaOH/Al_2O_3$.

In order to further explore the influence of H_2S on COS hydrolysis, the transient experiment of COS hydrolysis was carried out, and the results are shown in Figure 7a. In the absence of H_2S, the hydrolysis efficiency of COS on γ-Al_2O_3, $NaOH/Al_2O_3$, and KOH/Al_2O_3 catalysts are 87, 98, and 97%, respectively. In the presence of H_2S for 6 h, the hydrolysis efficiency decreased to 67, 85, and 82%, respectively. When the flow of H_2S is interrupted, the hydrolysis efficiency continues to decline on γ-Al_2O_3. The presence of H_2S in the COS hydrolysis reaction can accelerate the poisoning of the catalyst. If H_2S is stopped, the poisoning of the catalyst will still exist, indicating that the process of sulfur poisoning is irreversible. At the reaction temperature of 120 °C, sulfur deposition products will not decompose, and the amount of sulfur deposition increases with the increase of the reaction time. From Figure 7b, the breakthrough time for H_2S is 390 min on $NaOH/Al_2O_3$, much longer than that on γ-Al_2O_3 and KOH/Al_2O_3. The advantage of $NaOH/Al_2O_3$ is reflected in the reduction of sulfur deposition products and its high adsorption capacity for H_2S. Since the medium alkaline centers of $NaOH/Al_2O_3$ are obviously higher than that of the other two samples, it further proves that medium-strong alkaline centers are the adsorption site of H_2S, so $NaOH/Al_2O_3$ has stronger sulfur resistance.

To further explore the forms of sulfur species on the catalyst surface, three catalysts were pretreated in H_2S and H_2S + O_2 atmospheres, and then, thermogravimetric analysis was carried out. Since DTG characterization uses samples dried at 120 °C for 12 h, the effect of H_2O is not considered. The results are shown in Figure 8. The catalysts show significant weight loss peaks at 150−800 °C in the absence or presence of O_2. The release of SO_2 is mainly due to the decomposition of sulfite and sulfate, and the desorption of H_2S is mainly in the form of chemical adsorption. Since the sulfur vapor from the sublimation of elemental sulfur is difficult to detect, the sulfur content was calculated by subtracting the contents of SO_2 and H_2S from the total weight loss based on the thermogravimetric curve. The total weight loss of $NaOH/Al_2O_3$ and KOH/Al_2O_3 catalysts is significantly higher than that of γ-Al_2O_3, due to the higher H_2S adsorption capacity. In the H_2S and O_2 coexisting atmosphere, the total weight loss of the three catalysts is about 1.5 times higher than that in the H_2S atmosphere, indicating that the presence of O_2 promotes sulfur deposition. In the H_2S atmosphere, the proportion of SO_2 produced by sulfate or sulfite decomposition exceeds 50% on the γ-Al_2O_3 catalyst, while the content of elemental sulfur is greatly increased in $NaOH/Al_2O_3$ and KOH/Al_2O_3 catalysts, which is basically consistent with the results in Figure 6. In the H_2S + O_2 atmosphere, the elemental sulfur content of the three samples decreased significantly while the sulfate content increased

https://doi.org/10.1021/acsomega.3c01811
ACS Omega 2023, 8, 35608−35618

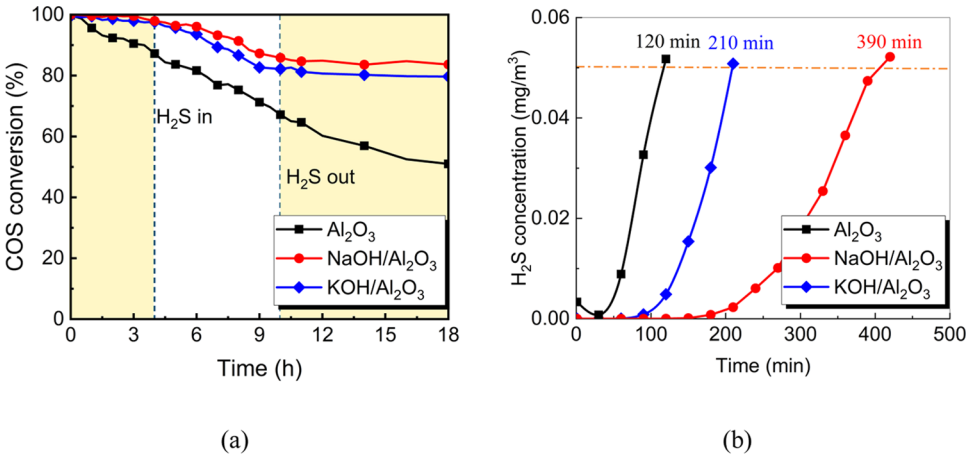

Figure 7. (a) Transient experiment of the H_2S effect on COS hydrolysis efficiency and (b) H_2S breakthrough curve.

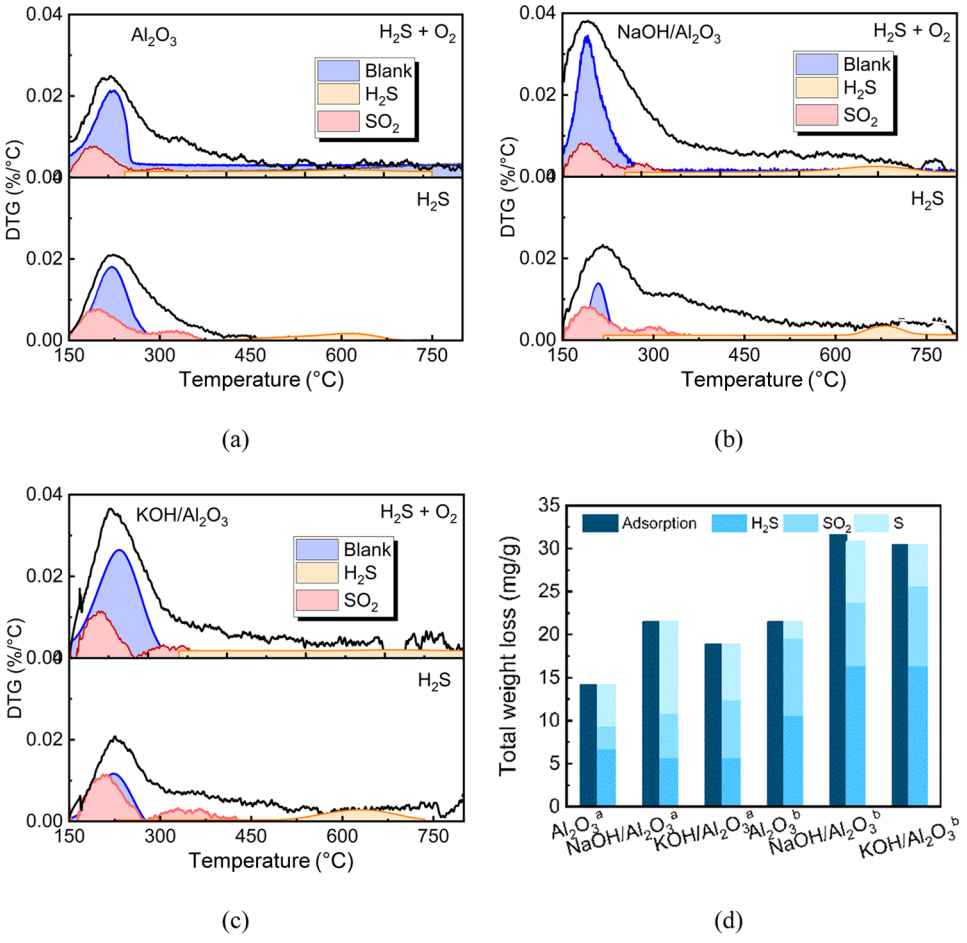

Figure 8. DTG curve of catalysts (a) γ-Al_2O_3, (b) $NaOH/Al_2O_3$, and (c) KOH/Al_2O_3; and (d) adsorption capacity and weight loss ([a] H_2S; [b] $H_2S + O_2$, "Blank" means unreacted sample weight loss).

significantly, indicating that the presence of O_2 increases the oxidation of sulfur.

3.4. Mechanism of COS Hydrolysis in the Presence of H_2S and O_2. In order to explore the mechanism of COS hydrolysis on alkali metal-supported γ-Al_2O_3 catalysts, in situ DRIFT tests were conducted in four atmospheres of N_2, H_2S, O_2, and $H_2S + O_2$. The results are shown in Figure 9. The adsorption peaks are as follows: −OH (3748−3740 cm^{-1}), H_2O (3427 cm^{-1}), CO_2 (2360 cm^{-1}), COS (2070 cm^{-1}), and HCO_3^- (1637 cm^{-1}—antisymmetric stretching vibration peak, 1412 cm^{-1}—symmetric stretching vibration peak), S^{2-} (1440 cm^{-1}), SO_4^{2-} (1128 cm^{-1}), HSO_3^- (995 cm^{-1}), and reaction intermediate $HSCO_2^-$ (1540 cm^{-1}). The wide adsorption peak of H_2O on γ-Al_2O_3, $NaOH/Al_2O_3$, and KOH/Al_2O_3 catalysts increases in N_2, H_2S, and O_2 atmospheres, indicating that the catalyst surface has a certain adsorption of H_2O and gaseous H_2O is continuously adsorbed on the catalyst surface to ensure efficient hydrolysis. The adsorption peaks of $HSCO_2^-$

https://doi.org/10.1021/acsomega.3c01811
ACS Omega 2023, 8, 35608−35618

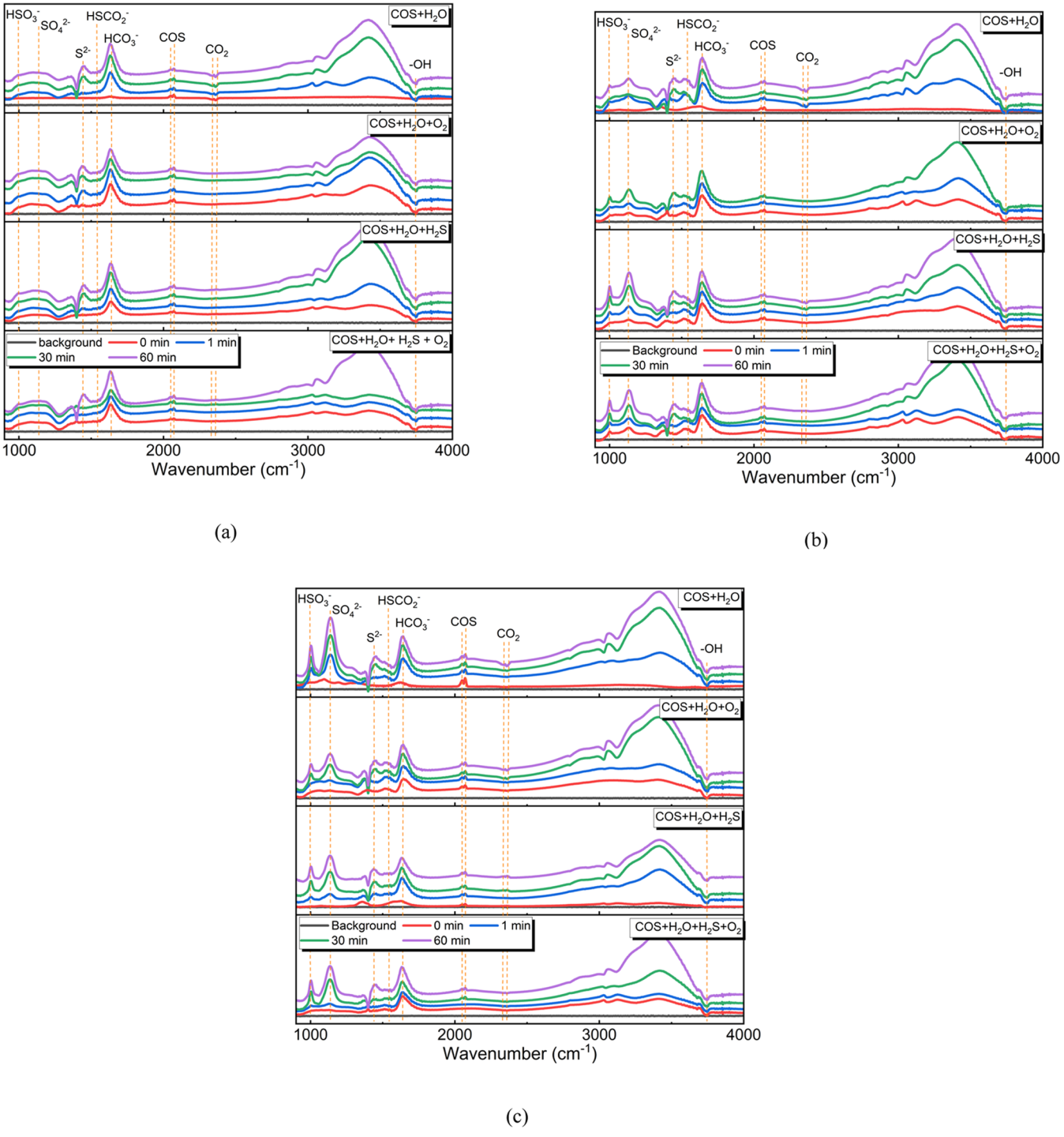

Figure 9. DRIFT spectrum of catalysts (a) γ-Al_2O_3, (b) $NaOH/Al_2O_3$, and (c) KOH/Al_2O_3.

appeared in the reaction under different atmospheres and catalysts, which proved that $HSCO_2^-$ was the intermediate product of the reaction.

In the atmosphere of COS + H_2O in Figure 9c, it can be clearly seen that the HSO_3^- and SO_4^{2-} amounts of the KOH/Al_2O_3 catalyst are the highest, while as shown in Figure 9b, the S^{2-} amount of the $NaOH/Al_2O_3$ catalyst is the highest, and the sediments of catalyst γ-Al_2O_3 are the least, which is consistent with the previous conclusion: the addition of alkali metals increased the strength of the alkaline center, resulting in the intensification of sulfur deposition. At the same time, the elemental sulfur was more easily produced on the $NaOH/Al_2O_3$ catalyst, and sulfur was further oxidized to sulfate and sulfite on the KOH/Al_2O_3 catalyst.

When H_2S or O_2 was added to the atmosphere, the reaction of the three catalysts was the same, that is, HSO_3^- and SO_4^{2-} amounts increased significantly, while S^{2-} amounts did not have obvious change. However, the mechanism of H_2S and O_2 is obviously different. The addition of H_2S increases the content of total sulfur, indicating that H_2S has no obvious oxidation effect on the generation of sulfur deposition but only increases the content of sulfate due to the increase of total

https://doi.org/10.1021/acsomega.3c01811
ACS Omega 2023, 8, 35608−35618

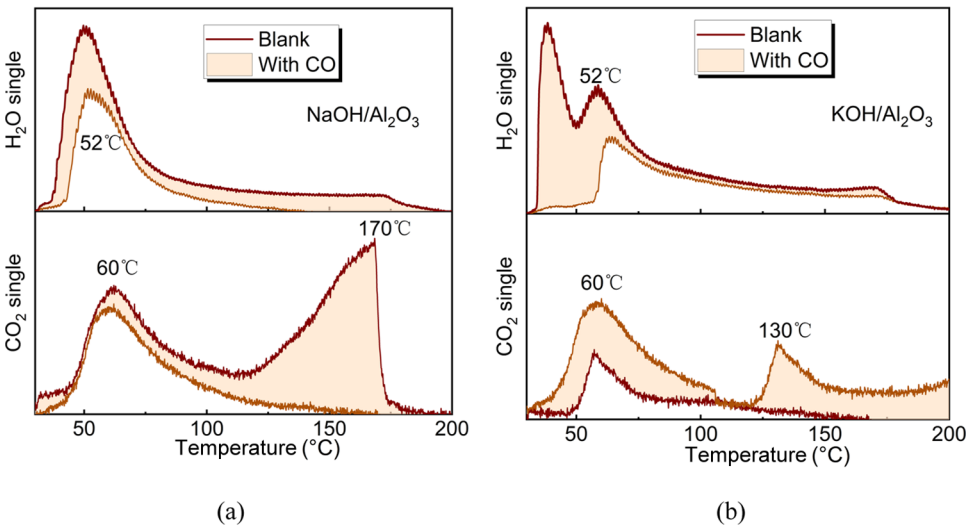

Figure 10. Analysis of CO oxidation products of catalysts (a) $NaOH/Al_2O_3$ and (b) KOH/Al_2O_3.

sulfur in the inlet. The addition of O_2 did not increase the total sulfur content in the inlet, but the total amount of sulfur deposition and the proportion of sulfate increased significantly, indicating that the presence of O_2 had an obvious oxidation effect on sulfur deposition.

Alkali metals Na and K have similar electronic structures, but the $NaOH/Al_2O_3$ catalyst show better sulfur resistance, which may be due to the different existing forms of Na and K on the catalyst surface. Therefore, the forms of the active components were investigated by mass spectrometry in a CO atmosphere, and the results are shown in Figure 10. Na and K may exist on the catalyst surface in the form of M−OH or M−O. In the presence of CO, it reacts with −OH and lattice oxygen to generate CO_2 and H_2O, and the reactions are shown in eqs 7 and 8. The proportion of M−OH can be determined by the signal of H_2O, and the proportion of M−O can be determined by the difference between the signal value of CO_2 and H_2O. The area of the blank curve represents the substrate value of the catalyst, and the shaded area represents the amount of H_2O and CO_2 produced after CO oxidation. According to the proportion of H_2O and CO_2 generated on the catalyst surface, the proportion of Na−O and NaOH on the $NaOH/Al_2O_3$ catalyst surface is about 65 and 35%, respectively. The proportion of K−O and KOH on the surface of the KOH/Al_2O_3 catalyst is about 30 and 70%, respectively. The $NaOH/Al_2O_3$ catalyst surface is dominated by Na−O, and the KOH/Al_2O_3 catalyst surface is dominated by KOH.

$$MO + CO \rightarrow CO_2 + M^+ \quad (7)$$

$$2MOH + CO \rightarrow CO_2 + H_2O + 2M^+ \quad (8)$$

Based on the above analysis, a possible COS hydrolysis mechanism is proposed, as shown in Figure 11. COS adsorbs on the weak alkaline center on the catalyst surface to generate intermediate product $HSCO_2^-$, which continues to react with the adsorbed H_2O to generate adsorbed H_2S and CO_2. The elemental sulfur is further oxidized to SO_4^{2-} on the surface of $NaOH/Al_2O_3$ under the action of Na−O and O_2, or elemental sulfur reacts with KOH on the surface of KOH/Al_2O_3 to form HSO_3^-, which is further oxidized to sulfate and deposited in the catalyst surface. The mechanism discussed in Figure 11 belongs to the alkali catalysis mechanism. Increasing the

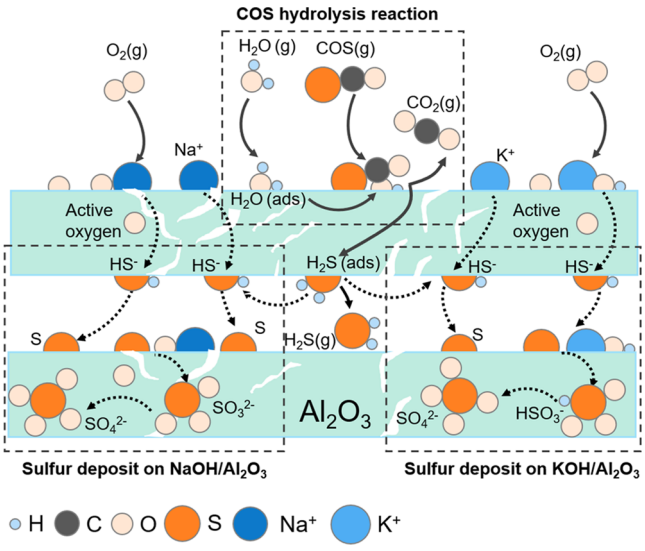

Figure 11. Mechanism of COS hydrolysis in the presence of H_2S and O_2.

proportion of strong alkaline centers on the catalyst surface is conducive to inhibiting the further oxidation of H_2S and improving the sulfur resistance of the catalyst. The understanding helps to develop better catalysts for removing COS from blast furnace gas.

4. CONCLUSIONS

The addition of alkali metals Na and K increases the strength of the weak alkali center on the catalyst surface, and the weak alkali center is the active center of the COS hydrolysis reaction, so the hydrolysis efficiency of the catalyst is significantly improved. COS adsorbs on the weak alkaline center on the catalyst surface to generate intermediate product $HSCO_2^-$, which continues to react with the adsorbed H_2O to generate adsorbed H_2S and CO_2; H_2S can be oxidized to elemental sulfur by free oxygen on the catalyst surface. The elemental sulfur is further oxidized to SO_4^{2-} on the surface of $NaOH/Al_2O_3$ under the action of Na−O and O_2, or elemental sulfur reacts with KOH on the surface of KOH/Al_2O_3 to form HSO_3^-, which is further oxidized to sulfate and deposited in

https://doi.org/10.1021/acsomega.3c01811
ACS Omega 2023, 8, 35608−35618

the catalyst surface. The main cause of catalyst sulfur poisoning is the presence of O_2, which intensifies both the total amount of sulfur deposition and the proportion of sulfate. The NaOH/Al_2O_3 catalyst shows better sulfur resistance than the KOH/Al_2O_3 catalyst for two reasons: first, the support of Na can significantly improve the medium-strong alkaline site, which is the adsorption site of H_2S. This is equivalent to increasing the "sulfur capacity" of H_2S adsorption and reducing the impact of sulfur deposition on the main reaction. Second, the sulfur was more easily produced on the NaOH/Al_2O_3 catalyst, and the sulfur was further oxidized to sulfate and sulfite on the KOH/Al_2O_3 catalyst. The molecular diameter of elemental sulfur is smaller than that of sulfate. Therefore, NaOH/Al_2O_3 catalyst has better sulfur resistance.

In this work, the relationship between the oxidation sites of H_2S and the alkaline centers of COS hydrolysis has been further revealed. Moreover, the effects of alkali metal species on the sulfur-containing species were illustrated. Increasing the content of medium-strong alkaline centers on the catalyst surface improves the sulfur capacity of the catalyst, and reducing the content of −OH groups inhibits further oxidation of H_2S. Therefore, much better catalysts can be developed by regulating the distribution of various alkaline centers.

AUTHOR INFORMATION

Corresponding Author

Yuran Li − *CAS Key Laboratory of Green Process and Engineering, Institute of Process Engineering, Innovation Academy for Green Manufacture, Chinese Academy of Sciences, Beijing 100190, China;* orcid.org/0000-0003-0131-9622; Email: yrli@ipe.ac.cn

Authors

Qiang Cao − *State Key Laboratory of Clean and Efficient Coal Utilization, Taiyuan University of Technology, Taiyuan 030024, China; CAS Key Laboratory of Green Process and Engineering, Institute of Process Engineering, Innovation Academy for Green Manufacture, Chinese Academy of Sciences, Beijing 100190, China*

Yuting Lin − *CAS Key Laboratory of Green Process and Engineering, Institute of Process Engineering, Innovation Academy for Green Manufacture, Chinese Academy of Sciences, Beijing 100190, China*

Jinglei Tian − *HBIS Group Co., Ltd., Shijiazhuang 050023, China*

Hongqiang Liu − *HBIS Group Co., Ltd., Shijiazhuang 050023, China*

Tingyu Zhu − *CAS Key Laboratory of Green Process and Engineering, Institute of Process Engineering, Innovation Academy for Green Manufacture, Chinese Academy of Sciences, Beijing 100190, China*

Jiancheng Wang − *State Key Laboratory of Clean and Efficient Coal Utilization, Taiyuan University of Technology, Taiyuan 030024, China*

Complete contact information is available at: https://pubs.acs.org/10.1021/acsomega.3c01811

Notes

The authors declare no competing financial interest.

ACKNOWLEDGMENTS

This work was supported by the "Clean Combustion and Low-carbon Utilization of Coal" Strategic Priority Research Program of the Chinese Academy of Sciences (No. XDA29000000), the Key Research and Development Program of Hebei Province (No. 21373702D), and the Key Science and Technology Program of HBIS Group Co., Ltd. (No. HG2021117).

REFERENCES

(1) Xu, W. Q.; Cao, W. J.; Zhu, T. Y.; Li, Y. J.; Wang, B. Material Flow Analysis of CO_2 Emissions from Blast Furnace and Basic Oxygen Furnace Steelmaking Systems in China. *Steel Res. Int.* **2015**, *86*, 1063−1072.

(2) Ahmed, H. New Trends in the Application of Carbon-Bearing Materials in Blast Furnace Iron-Making. *Minerals* **2018**, *8*, 561.

(3) Zhang, Q.; Xu, J.; Zhao, X. Y.; Wang, Y. J. Energy and Exergy Analyses of An Integrated Iron and Steel Making Process. *Int. J. Exergy* **2018**, *26*, 454−480.

(4) Bhaskar, A.; Assadi, M.; Somehsaraei, H. N. Decarbonization of the Iron and Steel Industry with Direct Reduction of Iron Ore with Green Hydrogen. *Energies* **2020**, *13*, 758.

(5) Chen, J. W.; Zhang, H.; Zhao, G.; Qureshi, A. S. A novel method for estimating carbon emission based on industrial metabolism: Blast furnace iron-making with micro mechanism model. *Energy Rep.* **2022**, *8*, 10125−10133.

(6) Chen, Z. G.; Deng, B. W.; Du, K. F.; Mao, X. H.; Zhu, H.; Xiao, W.; Wang, D. H. Flue-Gas-Derived Sulfur-Doped Carbon with Enhanced Capacitance. *Adv. Sustainable Syst.* **2017**, *1*, No. 1700047.

(7) Liu, X.; Zhangsun, G. Q.; Zheng, Y.; Liang, S. J.; Cao, Y. N.; Liu, F. J.; Xiao, Y. H.; Jiang, L. L. Hierarchical N-Doped Carbons Endowed with Structural Base Sites Toward Highly Selective Adsorption and Catalytic Oxidation of H_2S. *Ind. Eng. Chem. Res.* **2021**, *60*, 2101−2111.

(8) Li, C. M.; Zhao, S. Y.; Yao, X. L.; He, L.; Xu, S. M.; Shen, X. B.; Yao, Z. L. The Catalytic Mechanism of Intercalated Chlorine Anions as Active Basic Sites in MgAl-layered Double Jydroxide for Carbonyl Sulfide Hydrolysis. *Environ. Sci. Pollut. Res.* **2022**, *29*, 10605−10616.

(9) Wang, Y. F.; Ding, L.; Long, H. M.; Xiao, J. J.; Qian, L. X.; Wang, H. T.; Xu, C. B. Carbonyl Sulfur Removal from Blast Furnace Gas: Recent Progress, Application Status and Future Development. *Chemosphere* **2022**, *307*, No. 136090.

(10) Wang, Z.; Zhang, J. L.; An, G.; Liu, Z. J.; Cheng, Z. M.; Huang, J. J.; Zhang, J. W. Analysis on the Oversize Blast Furnace Desulfurization and a Sulfide Capacity Prediction Model Based on Congregated Electron Phase. *Metall. Mater. Trans. B* **2016**, *47*, 127−134.

(11) Gupta, A. K.; Ibrahim, S.; Shoaibi, A. A. Advances in Sulfur Chemistry for Treatment of Acid Gas. *Prog. Energy Combust.* **2016**, *54*, 65−92.

(12) Gao, P. T.; Li, Y. R.; Lin, Y. T.; Chang, L. P.; Zhu, T. Y. Promoting Effect of Fe/La Loading on γ-Al_2O_3 Catalyst for Hydrolysis of Carbonyl Sulfur. *Environ. Sci. Pollut. Res.* **2022**, *29*, 84166−84179.

(13) Nimthuphariyha, K.; Usmani, A.; Grisdanurak, N.; Kanchanatip, E.; Yan, M.; Suthirakun, S.; Tulaphol, S. Hydrolysis of Carbonyl Sulfide over Modified Al_2O_3 by Platinum and Barium in a Packed-bed Reactor. *Chem. Eng. Commun.* **2021**, *208*, 539−548.

(14) Cao, R.; Ning, P.; Wang, X. Q.; Wang, L. L.; Ma, Y. X.; Xie, Y. B.; Zhang, H.; Qu, J. X. Low-temperature Hydrolysis of Carbonyl Sulfide in Blast Furnace Gas Using Al_2O_3-based Catalysts with High Oxidation Resistance. *Fuel* **2022**, *310*, No. 122295.

(15) Ali, H.; Kansal, S. K.; Saravanamurugan, S. Alumina-Supported Alkali and Alkaline Earth Metal-Based Catalyst for Selective Decarboxylation of Itaconic Acid to Methacrylic Acid. *ChemistrySelect* **2021**, *6*, 3352−3359.

(16) Cho, E. H.; Park, Y. K.; Park, K. Y.; Song, D.; Koo, K. Y.; Jung, U.; Yoon, W. R.; Ko, C. H. Simultaneous Impregnation of Ni and an Additive via One-step Melt-infiltration: Effect of Alkaline-earth Metal (Ca, Mg, Sr, and Ba) Addition on Ni/γ-Al_2O_3 for CO_2 Methanation. *Chem. Eng. J.* **2021**, *428*, No. 131393.

(17) Li, J.; Zhang, Q. J.; Zhao, Y. H.; Qi, P.; Shao, C. Alkaline Earth Metal Oxide Modification of Ni/Al_2O_3 for Hydrogen Production from the Partial Oxidation and Reforming of Dimethyl Ether. *React. Kinet. Mech. Catal.* **2017**, *122*, 1193−1202.
(18) Churikov, A.; Gamayunova, I. M.; Zapsis, K. V.; Churikov, M. A.; Ivanishchev, A. V. Influence of Temperature and Alkalinity on the Hydrolysis Rate of Borohydride Ions in Aqueous Solution. *Int. J. Hydrogen Energy* **2012**, *37*, 335−344.
(19) Li, Y. R.; Lin, Y. T.; Xu, Z. C.; Wang, B.; Zhu, T. Y. Oxidation Mechanisms of H_2S by Oxygen and Oxygen-containing Functional Groups on Activated Carbon. *Fuel Process. Technol.* **2019**, *189*, 110−119.
(20) Li, K. L.; Wang, C.; Ning, P.; Li, K.; Sun, X.; Song, X.; Mei, Y. Surface Characterization of Metal Oxides-supported Activated Carbon Fiber Catalysts for Simultaneous Catalytic Hydrolysis of Carbonyl Sulfide and Carbon Disulfide. *J. Environ. Sci.* **2020**, *96*, 44−54.
(21) Sun, K.; Shao, Y. W.; Li, Q. Y.; Liu, Q. H.; Wu, W. B.; Wang, Y.; Hu, S.; Xiang, J.; Liu, Q.; Hu, X. Cu-based Catalysts for Hydrogenation of 5-hydroxymethylfurfural: Understanding of the Coordination between Copper and Alkali/alkaline Earth Additives. *Mol. Catal.* **2019**, *474*, 110407.
(22) Pérez-Martínez, D. J.; Eloy, P.; Gaigneaux, E. M.; Giraldo, S. A.; Centeno, A. Study of the Selectivity in FCC Naphtha Hydrotreating by Modifying the Acid-base Balance of CoMo/gamma-Al_2O_3 Catalysts. *Appl. Catal., A* **2010**, *390*, 59−70.
(23) Dasireddy, V. D. B. C.; Stefancic, N. S.; Hus, M.; Likozar, B. Effect of Alkaline Earth Metal Oxide (MO) Cu/MO/Al_2O_3 Catalysts on Methanol Synthesis Activity and Aelectivity via CO_2 Reduction. *Fuel* **2018**, *233*, 103−112.
(24) Huang, H. M.; Yong, N.; Williams, B. P.; Taylor, S. H.; Hutchings, G. High Temperature COS Hydrolysis Catalyzed by Gamma-Al_2O_3. *Catal. Lett.* **2006**, *110*, 243−246.
(25) Rhodes, C.; Riddel, S. A.; West, J.; Williams, B. P.; Hutchings, G. J. The Low-temperature Hydrolysis of Carbonyl Sulfide and Carbon Disulfide: a Review. *Catal. Today* **2000**, *59*, 443−464.
(26) Gu, J.-n.; Liang, J.; Hu, S.; et al. Enhanced Removal of COS From Blast Furnace Gas via Catalytic Hydrolysis over Al_2O_3-based Catalysts: Insight into the Role of Alkali Metal Hydroxide. *Sep. Purif. Technol.* **2022**, *295*, No. 121356.
(27) Sun, X.; Ning, P.; Tang, X. L.; Yi, H. H.; Li, K.; He, D.; Xu, X. M.; Huang, B.; Lai, R. Y. Simultaneous Catalytic Hydrolysis of Carbonyl Sulfide and Carbon Disulfide over Al_2O_3-K/CAC Catalyst at Low Temperature. *J. Energy Chem.* **2014**, *23*, 221−226.
(28) Rupp, E. C.; Granite, E. J.; Stanko, D. C. Catalytic Formation of Carbonyl Sulfide during Warm Gas Clean-up of Simulated Coal-derived Fuel Gas with Pd/γ-Al_2O_3 Sorbents. *Fuel* **2012**, *92*, 211−215.
(29) Jin, H. K.; An, Z.; Li, Q. C.; Duan, Y. Q.; Zhou, Z. H.; Sun, Z. K.; Duan, L. B. Catalysts of Ordered Mesoporous Alumina with a Large Pore Size for Low-Temperature Hydrolysis of Carbonyl Sulfide. *Energy Fuels* **2021**, *35*, 8895−8908.
(30) Wang, L.; Wang, S. D.; Yuan, Q.; Lu, G. Z. COS Hydrolysis in the Presence of Oxygen: Experiment and Modeling. *J. Nat. Gas Chem.* **2008**, *17*, 93−97.
(31) Liu, N.; Ning, P.; Sun, X.; Wang, C.; Song, X.; Wang, F.; Li, K. Simultaneous Catalytic Hydrolysis of HCN, COS and CS_2 over Metal-modified Microwave Coal-based Activated Carbon. *Sep. Purif. Technol.* **2021**, *259*, No. 118205.
(32) Kamp, E.; Thielert, H.; von Morstein, O.; Kureti, S.; Schreiter, N.; Repke, J. U. Investigation on the Simultaneous Removal of COS, CS_2 and O_2 from Coke Oven Gas by Hydrogenation on a Pd/Al_2O_3 Catalyst. *Catal. Sci. Technol.* **2020**, *10*, 2961−2969.
(33) Liang, M. S.; Li, C. H.; Guo, H. X.; Xie, K. C.; Chu, J. L. Study of COS Hydrolysis Reaction Kinetics at Lower Temperature and in the Presence of CO_2. *J. Fuel Chem. Technol.* **2003**, *31*, 149−155.
(34) Palma, V.; Barba, D.; Gerardi, V. Honeycomb-structured Catalysts for the Selective Partial Oxidation of H_2S. *J. Cleaner Prod.* **2016**, *111*, 69−75.
(35) El Gamal, M. M.; El-Dieb, A. S.; Mohamed, A. M. O.; Sawy, K. M. Performance of Modified Sulfur Concrete Exposed to Actual Sewerage Environment with Variable Temperature, Humidity and Gases. *J. Build. Eng.* **2017**, *11*, 1−8.
(36) Shangguan, J.; Zhao, Y. S.; Fan, H. L.; Liang, L. T.; Shen, F.; Miao, M. Q. Desulfurization Behavior of Zinc Oxide Based Sorbent Modified by the Combination of Al_2O_3 and K_2CO_3. *Fuel* **2013**, *108*, 80−84.
(37) Liu, Y. L.; Wu, P.; Shen, K.; Zhang, Y. P.; Li, G. B.; Li, B. Contribution of Na/K Doping to the Activity and Mechanism of Low-Temperature COS Hydrolysis over TiO_2-Al_2O_3 Based Catalyst in Blast Furnace Gas. *ACS Omega* **2022**, *7*, 13299−13312.
(38) Yi, H. H.; Zhao, S. Z.; Tang, X. L.; Ning, P.; Wang, H. Y.; He, D. Influence of Calcination Temperature on the Hydrolysis of Carbonyl Sulfide over Hydrotalcite-derived Zn-Ni-Al Catalyst. *Catal. Commun.* **2011**, *12*, 1492−1495.
(39) Zhao, S. Z.; Yi, H. H.; Tang, X. L.; Song, C. Y.; et al. Low Temperature Hydrolysis of Carbonyl Sulfide Using Zn-Al Hydrotalcite-derived Catalysts. *Chem. Eng. J.* **2013**, *226*, 161−165.
(40) Zhao, S. Z.; Yi, H. H.; Tang, X. L.; Kang, D. J.; Gao, F. Y.; Wang, J. G.; Huang, Y. H.; Yang, Z. Y. Calcined ZnNiAl Hydrotalcite-like Compounds as Bifunctional Catalysts for Carbonyl Sulfide Removal. *Catal. Today* **2019**, *327*, 161−167.

https://doi.org/10.1021/acsomega.3c01811
ACS Omega 2023, 8, 35608−35618